Journal of Dental Sciences (2017) 12, 319–327

Available online at www.sciencedirect.com

ScienceDirect

journal homepage: www.e-jds.com

Original Article

Oxide layer characteristics and interfacial analysis of porcelain fused to high-gold alloy using multitechnique analysis methods

Hao-Sheng Chang [ab*†], Yu-Chun Chiu [a], Chao-Sen Yang [c], Ming Chen [c*†]

[a] Department of Dentistry, Kaohsiung Veteran General Hospital, Kaohsiung, Taiwan
[b] Department of Dental Technology, Shu Zen College of Medicine and Management, Kaohsiung, Taiwan
[c] Department of Materials and Optoelectronic Science, National Sun Yat-sen University, Kaohsiung, Taiwan

Received 30 December 2016; Final revision received 8 February 2017
Available online 4 April 2017

KEYWORDS
electron probe microanalysis;
gold–platinum alloy;
scanning electron microscopy combined with energy-dispersive X-ray analysis;
X-ray photoelectron spectroscopy

Abstract *Background/purpose:* In a previous fractural study, high-gold crowns possessed the second highest fracture force. The objective of this study is to analyze the interface of porcelain fused to high-gold alloy using different observation devices.
Materials and methods: High-gold crowns specimens with the morphology of a maxillary second premolar were compressed vertically in the center of the occlusal surface until fracture using a universal testing machine. The fractured surfaces were examined using scanning electron microscopy combined with energy-dispersive X-ray spectroscopy (SEM/EDX) to determine the failure mode. The ceramic–metal interface of the crown was examined with electron probe microanalysis (EPMA). In addition, sheet specimens with dimensions of $10 \times 9 \times 4$ mm^3 were prepared to examine the surface morphology and composition of high-gold alloy after oxidation using X-ray photoelectron spectrometer (XPS).
Results: The average fracture force was 1368 ± 312 N. Photograph of fractured crown and SEM/EDX analyses reveal that the crown initially suffered from cohesive failure in the upper and middle regions, with the fracture occurring mostly within the ceramic. XPS results and both EPMA color photomicrographs of crown and sheet specimens show that indium was observed along the porcelain–metal interface with a 1- to 2-μm disrupted zone of oxide layer.
Conclusion: In_2O_3 and Au were found along the interface from the multitechnique analysis methods; the presence of this oxide at the boundary promotes ceramic–metal adhesion.

* Corresponding authors. Department of Dentistry, Kaohsiung Veteran General Hospital, 386 Dazhong First Road, Kaohsiung 81362, Taiwan (H.-S. Chang); Department of Materials and Optoelectronic Science, National Sun Yat-sen University, 70 Lien-Hai Road, Kaohsiung 80424, Taiwan (M. Chen).
E-mail addresses: hschang1001@yahoo.com.tw (H.-S. Chang), mingchen@faculty.nsysu.edu.tw (M. Chen).
† H.-S.C. and M.C. contributed equally to this work.

http://dx.doi.org/10.1016/j.jds.2017.03.003

In_2O_3 is suggested to be beneficial for the second highest fracture resistance in a previous fractural study of implant-supported crowns.

Introduction

Dental implants can effectively restore the function of missing teeth, and are an active area of research.[1,2] In contrast to natural teeth, a dental implant has no periodontal ligament with the surrounding bone. The resulting poor capacity for the detection of occlusal forces increases the tendency for overloading, which in turn can result in peri-implant bone loss and implant failure.[3] Occlusal overloading is usually associated with a parafunctional habit or with premature contacts between an implant-supported crown and the opposing natural teeth or implant prostheses. Animal studies investigating the influence of occlusal overloading on peri-implanted bones revealed that occlusal overloading is an important factor in the loss of the osseointegration that occurs with dental implants.[3,4] The occlusal overloading-associated fracture of porcelain veneers is the most common complication for implant prostheses. For several decades, porcelain-fused-to-metal (PFM) crown has been used to restore partially or fully edentulous patients because of aesthetic necessity. However, a porcelain fracture, related to implant-supported PFM crowns or bridges, is a significantly greater risk than it is in tooth-supported restorations.[5] For long-term maintenance in oral condition, interfacial bonding and corrosive resistance between porcelain and alloy are very important.[6] The basic requirements for strong interfacial bonding of dental ceramometal systems are chemical bond and minimal stress concentration at the interfaces. Previous studies have reported that changes in the morphology of the oxidation zone and quantities of oxide for noble ceramometal alloys containing some base metals (In and Sn) play an important role in increasing the adherence of porcelain to noble alloys.[7–10]

It was previously thought that biological or mechanical factors were the dominant causes of failure after PFM crown restoration.[11] Studies using three or four points, and double bending tests to measure bonding strength between porcelain and metal coping were unable to accurately imitate the failure mode of a PFM crown under actual oral conditions.[12,13] Many PFM crown restoration casts were developed and the universal testing machine (MTS Systems Corp, Eden Prairie, MN, USA) was introduced to determine PFM crown fracture resistance.[14,15] In a recent fractural study of implant-supported crowns that were porcelain-fused to five different commercial alloys,[16] it was determined that the high-gold alloy had the second highest fracture force. The present study was one of the series of research, which tried to analyze and observe the interface characteristics of porcelain fused to high-gold alloy after firing cycles using multitechnique analysis methods, including X-ray photoelectron spectroscopy (XPS), scanning electron microscopy combined with energy-dispersive X-ray analysis (SEM/EDX), and electron probe microanalysis (EPMA), for characterizing the alloy surface after oxidation and the ceramic–metal interface after PFM firing cycles. Failure modes of fractured surfaces were determined using SEM/EDX and EPMA.

Materials and methods

Specimen preparation

The materials used in this study were Au–Pt dental casting alloys (Aquarius, Ivoclar Vivadent AG, Schann, Principality of Liechtenstein) with compositions shown in Table 1 (Column 2). In addition to the nominal alloy composition of 86.0 Au–11.0 Pt–2.5 In (wt%), Sn, Ta, Ir, and Li were present as trace elements (each <1 wt%). Uniform ceramometal crowns of an Au–Pt alloy, with equivalent morphologies to the maxillary second premolar, were duplicated on a Straumann straight screw-retained abutment (Lot No.: 048.605; Basel, Switzerland) connected to a Straumann regular neck tissue-leveled implant analog (Lot No.: 048.124) under a 35-N preload. In addition, Au–Pt alloy sheets with a dimension of $10 \times 9 \times 4$ mm^3 were prepared. Ten ceramometal crowns and six sheets of Au–Pt alloy were fabricated according to the manufacturer's instructions, involving five standard dental preparation stages (Figure 1).[17] For brevity, the detailed preparation stages and observation methods presented in the Pd–Ag article are not repeated here.[17]

1. Wax patterns were prepared, sprued, and invested. The alloy was melted, cast into the mold, and then bench-cooled.

Table 1 Bulk composition of Au–Pt alloy as supplied by the manufacturer, surface composition obtained from EDX and XPS analyses after surface oxidation of the alloy, and surface composition of fractured crown on alloy side (in wt %).

	M	EDX	XPS	Upper [a]	Middle [a]	Lower [a]
Au	86.0	58.5	31.6	0.0	0.0	38.2
Pt	11.0	7.5	3.8	0.0	0.0	0.0
In	2.5	34.0	64.6	0.0	0.0	61.8

Compositional data are expressed in wt% by adopting the sum of Au, Pt, and In as 100 wt%.
EDX = energy-dispersive X-ray analysis; M = manufacturer; XPS = X-ray photoelectron spectroscopy.
[a] Obtained from EDX analysis on three different areas along the fracture path.

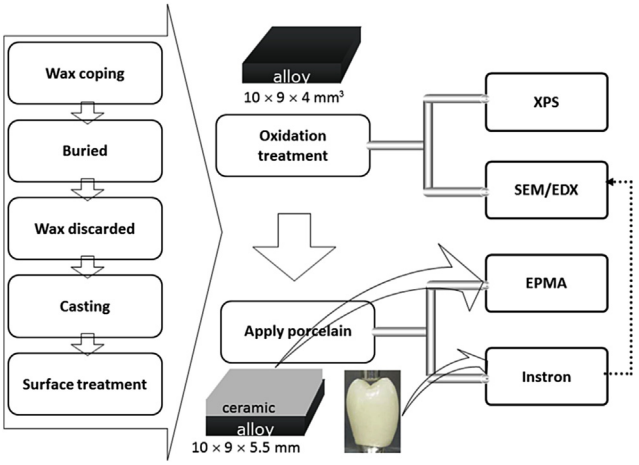

Figure 1 Schematic illustration of procedures for fabrication of rectangular specimens and crowns.[17] Corresponding characterization is shown on the right side. EDX = energy-dispersive X-ray analysis; EPMA = electron probe microanalysis; SEM = scanning electron microscopy; XPS = X-ray photoelectron spectroscopy.

2. After devesting, the alloy was blasted with 50-μm Al_2O_3 particles.
3. Specimens were grounded smoothly and were blasted again with 50-μm Al_2O_3 particles, and then the blasted surface was cleaned with steam.
4. After surface treatment, the specimens were oxidized by heating them in a mild vacuum (10 mmHg) in a dental ceramic furnace from 450°C to 1000°C at a rate of 45°C/min with a 1-minute hold at the peak temperature. The specimens were bench cooled to room temperature (RT). Three of these sheet specimens were left in this oxidized state. Their surfaces were first examined with XPS. SEM/EDX was then used to analyze the surface morphology and composition of these three specimens.
5. Fabrication of the crowns used eight PFM firing cycles. Two layers of opaque dental porcelain, with a combined thickness of 0.4 mm, were fired onto the crown surfaces. Three layers of dentin porcelain, with a combined thickness of approximately 1.0 mm, were fired onto the crowns. The crowns were bench set at RT after each firing cycle. The total porcelain thickness was approximately 1.4 mm. Two layers of glaze were fired onto the crowns, and the completed crowns were allowed to cool to RT.
6. A layer of approximately 0.5-mm opaque dental porcelain and then a layer of approximately 1.0-mm dentin porcelain were PFM fired onto the other three sheet specimens. These three specimens were bench set at RT in each firing cycle. Each specimen with a cross section of 9×5.5 mm^2 was embedded in a resin that was cured from a mixture of conducting mounting compound and epoxy mounting powder. The mounted specimens were mechanically polished by sequentially using a series of SiC papers, and additionally polished by diamond pastes, leaving a mirror finish. The surfaces were then carefully cleaned and air dried. Distribution of elements around the interface of ceramic and alloy after two PFM firing cycles was examined using EPMA.

Compressive fracture testing

Compressive fracture tests of ceramometal crowns were performed using a universal testing machine.[16,17] Figure S1[17] in the supplementary material online photographically shows a custom-built loading apparatus following the design of Torrado et al.[15] The upper member of the apparatus consisted of a 15-mm-diameter hardened stainless steel shaft that connected to the end of the loading part of the universal testing machine. The opposite end of the shaft was machined to house a 3-mm-diameter loading pin with rounded edges. Only the loading pin contacted the porcelain during testing, and a new pin was used to load each crown. The crown was set on the abutment-analog model mounted on the lower part of the testing machine. An axial load was applied to the inner inclination of buccal and lingual cusps of the occlusal table at the same distance from the central groove. Specimens were subjected to a vertical compressive load at a crosshead speed of 0.5 mm/min until failure to obtain the ultimate fractural strength.

X-ray photoelectron spectroscopy

The outermost part of the oxidized sheet specimens was subjected to XPS analysis using a JAMP-9500F photoelectron spectrometer (JEOL, Tokyo, Japan). An Al Kα X-ray source (1486.6 eV) was obtained using a 10-kV accelerating voltage and a 10-mA filament current. The measured binding energies (BEs) were calibrated by referencing the BE of the C 1s line of hydrocarbon contamination (285.0 ± 0.2 eV).[18] The weight percentages of Au, Pt, and In on the surface area of the oxidized specimens were calculated according to the relative peak areas, and corrected using Wagner's atomic sensitivity factors.[19]

Scanning electron microscopy/energy-dispersive X-ray analysis

The fracture surfaces on both sides of the failed crowns were sputter coated with carbon to produce a thin conductive layer. The oxidized sheet specimens were also coated with carbon following XPS analysis. Morphological features of these specimens were examined using a field emission SEM JSM-6330TF (JEOL). An EDX spectrometer incorporated into the SEM was used to characterize the elemental composition. EDX spectra were collected from the upper, middle, and lower regions on both sides of the failed crowns, or from different regions of each sheet specimen using an area scan mode. Quantitative EDX area analysis was executed to determine the weight percentage values of Au, Pt, In, Si, Zr, Al, K, and Na, and to calculate the mean values of Au, Pt, and In.

Electron probe microanalysis

A cross-sectioned crown was embedded in resin cured from a mixture of conducting mounting compound and epoxy mounting powder. The mounted crown was mechanically polished using the same procedures as described for the sheet specimens. These metallographically polished

specimens were coated with carbon. The backscattered electron image (BEI) was taken over an area of 66×66 μm^2 (1500×) by a JEOL JXA-8900R EPMA at 15 kV. For elemental mapping, the electron beam was scanned over an area of 66×39 μm^2, and simultaneously characteristic X-ray intensities of the corresponding elements were acquired. Elemental concentration profiles in the cross-sectional layer of the ceramic and metal interface were measured using a 1-μm-diameter beam.

Results

Figure 2 shows the load–displacement plots acquired during the fracture testing. The maximum load corresponds to the onset of a catastrophic fracture of the crown. Nine load and displacement paired values are listed with plot symbols. The average fractural force was 1368 ± 312 N. A photograph of the fracture surfaces of a representative ceramometal crown is presented in Figure 3. Arrows show the localized areas in filled circles that were analyzed by EDX. The majority of fractures occur in the opaque porcelain layers along the upper and middle regions of the crown, with some porcelain remnants being present on the alloy surface.

In Figure S2 in the supplementary material online, the three representative BEI micrographs (upper, middle, and lower) and the elemental EDX area scans of the fracture surface on the alloy side show the Zr, Si, K, Al, Na, Au, and In peaks. Figure S3 in the supplementary material online illustrates three representative BEI micrographs (upper, middle, and lower) and the elemental EDX area scans of the fracture surface on the porcelain side. This figure shows the Zr, Si, K, Al, Na, Au, and Pt peaks. The elemental composition of the crown's fractural surfaces obtained by EDX analysis is listed in Table 2. Au, Pt, and In were not detected on both sides of the fracture crowns in the upper and middle regions. In was not detected on the porcelain side of the fracture and no Pt was found on the alloy side, indicating that the fracture occurred along the interfacial oxide layer in the lower region. The observed composition may not represent a surface phenomenon because the overall depth sampled by EDX is approximately 1 μm. The crown initially suffered from cohesive failure, with the fracture occurring mostly within the ceramic. The schematic diagram shown in Figure 4 uses solid lines to represent the crack path. The initial crack started at the 3-mm-diameter loading pin–crown interface, propagated through the dentin porcelain layers, and spread into the opaque porcelain layers. Finally, the crown fractured as the crack approached the oxide layer and the bulk of Au–Pt alloy.

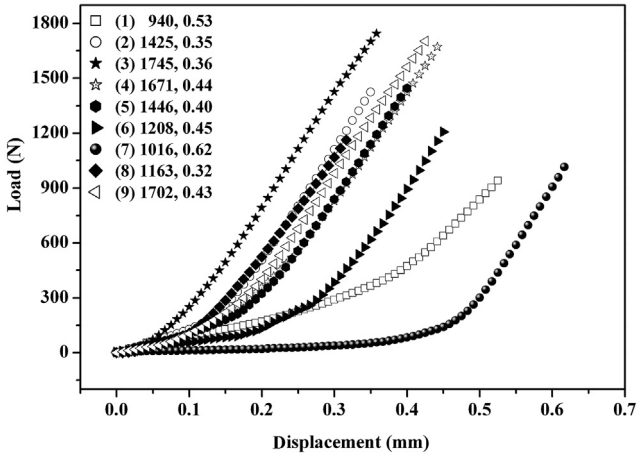

Figure 2 Load against displacement curves from fracture testing.

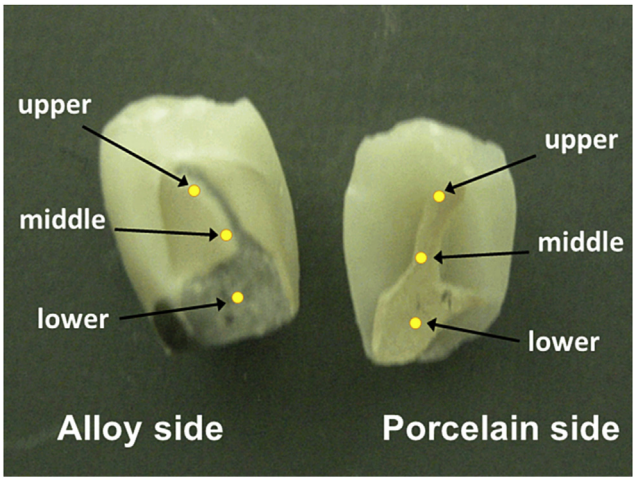

Figure 3 Representative photograph of fractured crown. Arrows show upper, middle, and lower areas for scanning electron microscopy/energy-dispersive X-ray analysis.

EPMA was employed to scan the elemental distribution mappings in the metallographically polished crown. A compositional contrast between the alloy and porcelain phases was observed using a backscattering electron detector (Figure 5A). Au, In, and Pt compositions are shown in Figures 5B–5D, respectively. Au and In elements are presented on the alloy side of the specimens, although a more intense In signal is seen along the ceramic–metal boundaries. Pt was not observed along the ceramic–metal boundaries, and weak Pt signal was detected in the alloy side. The figure shows a rough surface structure along the ceramic–metal boundaries.

Figure 6 displays a typical survey scan over a BE range of 0–1400 eV for the Au–Pt alloy after surface oxidation. This

Table 2 Surface compositions of fractured crown (in wt %).

	Upper area		Middle area		Lower area	
	Alloy side	Porcelain side	Alloy side	Porcelain side	Alloy side	Porcelain side
Au	0.0	0.0	0.0	0.0	20.6	28.9
Pt	0.0	0.0	0.0	0.0	0.0	29.9
In	0.0	0.0	0.0	0.0	33.3	0.0
Si	34.0	34.3	36.3	32.7	12.7	23.2
Zr	40.9	38.5	33.9	39.8	20.4	0.0
Al	8.7	9.4	9.9	8.6	4.4	5.7
K	12.0	11.5	13.6	12.1	5.2	9.1
Na	4.5	6.4	6.3	6.8	3.5	3.3

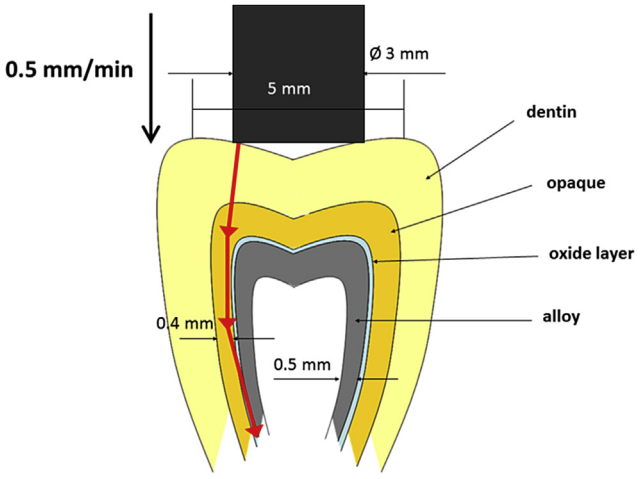

Figure 4 Schematic illustration of the crack path.

spectrum reveals the presence of Au, In, and Pt. Their weight concentrations (wt%) based on curve fitting analysis are listed in Column 4 of Table 1. A narrow scan of the In 3d line is shown in Figure 7. The main peak at approximately 444.2 eV corresponds to In_2O_3.[18–20] After deconvolution of this In 3d line, no peak was detected at 443.5 eV that corresponds to the In 3d BE in metallic In.[19,20]

Figure S4 in the supplementary material online presents secondary electron image micrographs for the oxidized alloy surface. Irregular rough surface characteristics are observed under different magnifications. Figure S5 in the supplementary material online illustrates a representative BEI micrograph and its elemental EDX area scan of the oxidized sheet specimen, which shows the Au and Pt peaks from a ~1-μm particle. The results of EDX analysis on the elemental composition of the alloy surfaces are presented in the third column of Table 1. The BEI micrograph and elemental EDX scans for the oxidized alloy are presented in Figure 8. Elemental EDX maps indicate that all the elements of In, Au, and Pt are evenly distributed over the surface of the specimens. The observed homogeneous distribution is not necessarily a surface phenomenon because the overall depth sampled by EDX is of the order of 1 μm.

The EPMA method was used to scan the elemental distribution mappings of the metallographically polished sheet specimens after two PFM firing cycles. The compositional contrast between the metal and porcelain phases was observed using a backscattered detector, as presented in Figure 9A. The results of Au, In, and Pt are illustrated in Figures 9B–9D, respectively. Au, In, and Pt elements were distributed only on the metal side of the specimens, and more intense In signal was detected along the metal–porcelain boundaries as compared with Au and Pt. These micrographs indicate that the oxidized specimens have a rough surface structure, which is also observed in the secondary electron image micrographs of Figure S4 in the supplementary material online.

Discussion

Owing to the sampling depth of XPS, chemical information is acquired selectively from an ultra-thin layer (a few nanometers) on the alloy surface. Surface sensitivity is an advantage of XPS. The problem with SEM/EDX measurements is that the sampled volume is approximately 1 μm in diameter, which prevents extremely thin external oxide layers from being detected. The main advantage of SEM/EDX is that it exhibits favorable spatial resolution. Columns 3 and 4 in Table 1 show the mean compositional data based

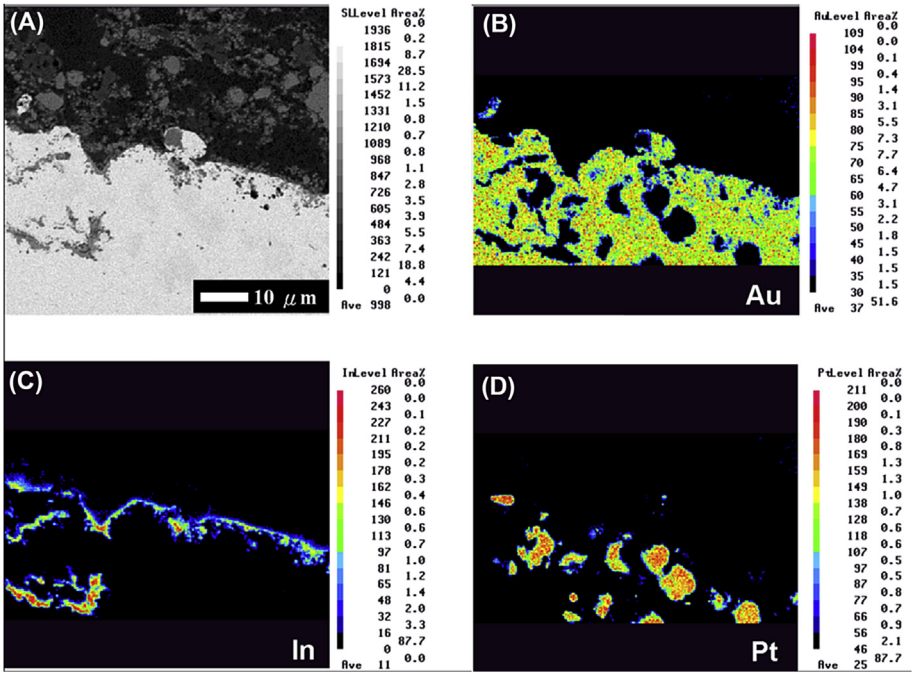

Figure 5 (A) Backscattered electron image micrograph, and electron probe microanalysis color photomicrographs showing element distributions of (B) Au, (C) In, and (D) Pt around the interface within the crown.

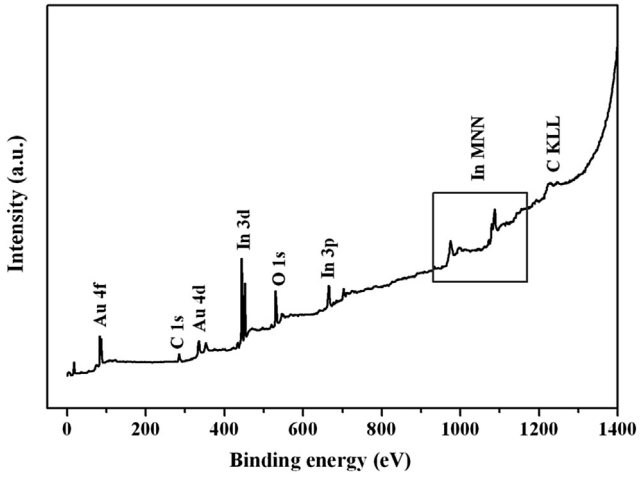

Figure 6 X-ray photoelectron spectroscopy wide scan of alloy after surface oxidation.

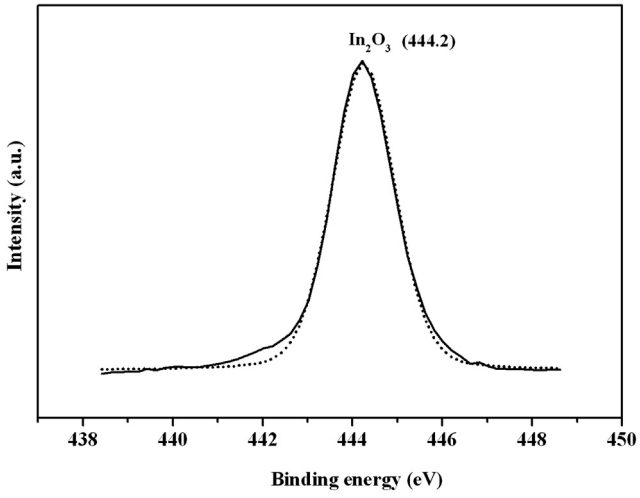

Figure 7 X-ray photoelectron spectroscopy narrow scan of alloy after surface oxidation showing In $3d_{5/2}$ peak spread over 439–448 eV and covering In^0 and In_2O_3.

on the EDX and XPS analysis of the Au–Pt alloy after surface oxidation, as compared with the bulk composition information (Column 2) provided by the manufacturer. The compositional data are expressed in wt% by adopting the sum of Au, Pt, and In as 100%. The EDX and XPS measurements qualitatively showed a decrease in the Au (from 86.0 wt% to 58.5 wt% to 31.6 wt%) and Pt (from 11.0 wt% to 7.5 wt% to 3.8 wt%) contents after surface oxidation. By contrast, a growing concentration of In (from 2.5 wt% to 34.0 wt% to 64.6 wt%) content was detected. Performing quantification using a sufficient statistical value was not possible because it would have required a higher number of measurements. The most noticeable change to the specimens after oxidization is the Au and Pt elements being major components (86.0 + 11.0 wt%) in the bulk, but only approximately 35 wt% (31.6 + 3.8) appearing on the surface. The EPMA micrograph also indicates that more intense In element is along the metal–porcelain boundaries.

In Figure 6, the measured BE of Au is in good agreement with the reference data and remains unchanged after oxidation treatment,[18,19] as is expected for noble metal alloy. As shown in Figure 7, In was present as oxide In_2O_3. The near-surface accumulation of In_2O_3 may be caused by segregation of In from the bulk to the surface of the specimen and subsequent oxidation. This work confirms the research of Brantley et al.[21] who found that alloy surface preparation could have an effect on the surface elements present in the alloy oxide layer, particularly during the oxidation procedure. While firing the ceramic, the alloy was twice heated to 930°C, reentering a single-phase zone each time. Because of the high energy at high temperatures, the atoms are enabled to diffuse in the crystal lattice and forced to distribute randomly at the atomic sites (Figure 8). It has been proposed that the mechanism of the resulting enhanced oxide adherence arises from a reduction in the vacancy concentration at the metal–oxide interface.[22] The formation of metal–oxide top layers (In_2O_3) is essential in bringing elements to the surface that are directly involved in the metal–ceramic bond.

Besides the chemical bonding between porcelain and the alloy interface, micromechanical interlocking was also reported previously.[23–26] The advantages of blasting the alloy surface with Al_2O_3 particles, prior to porcelain application, are the increases in surface roughness and surface area. This process has been demonstrated to increase the metal–ceramic adherence.[27–29] The micrographs of SEM (Figure S4 in the supplementary material online) and EPMA (Figures 5 and 9) provide the possibility of mechanical interlocking in this study.

The average and minimum fracture forces (1368 ± 302 N and 940 N, respectively) for Au–Pt ceramometal crowns were substantially greater than the maximal molar region biting force of 847 N for men and 597 N for women.[9] We assumed that the interface conditions between the crown to abutment and implant analog provided fully intimate contact for the tested models. However, a completely passive interfacial fit does not usually occur in real clinical situations, and the screw designs and rough surfaces of dental implants are dissimilar to the abutment used in our model. These variables for a real dental implant may affect the efficiency of an occlusal load transfer to the surrounding bone, and may cause stress concentration in the occlusal table or at the connection of the abutment and dental implant.[30] Testing models have their limitations because the biomechanical properties and nonlinear behavior of biological tissues in a real oral cavity cannot be predicted precisely. In the laboratory, the use of a single-cycle load-to-failure and mouth-motion fatigue tests with simplified geometries will provide limited data for guiding the development of PFM systems.[10] However, the fracture surface and interface analyses conducted in this study are still vital for successful ceramometal restoration. We conclude that mechanical interlocking[27,31–33] contributes to the interface strength from the rough morphologies seen at the alloy–porcelain boundaries (Figures S4 in the supplementary material online and Figures 5 and 9, main text). Based on the results from EDX analysis and the observation that the fractural pathway remained mostly within the opaque porcelain layer, it is suggested that an adhesive bonding force between the alloy and ceramic is greater

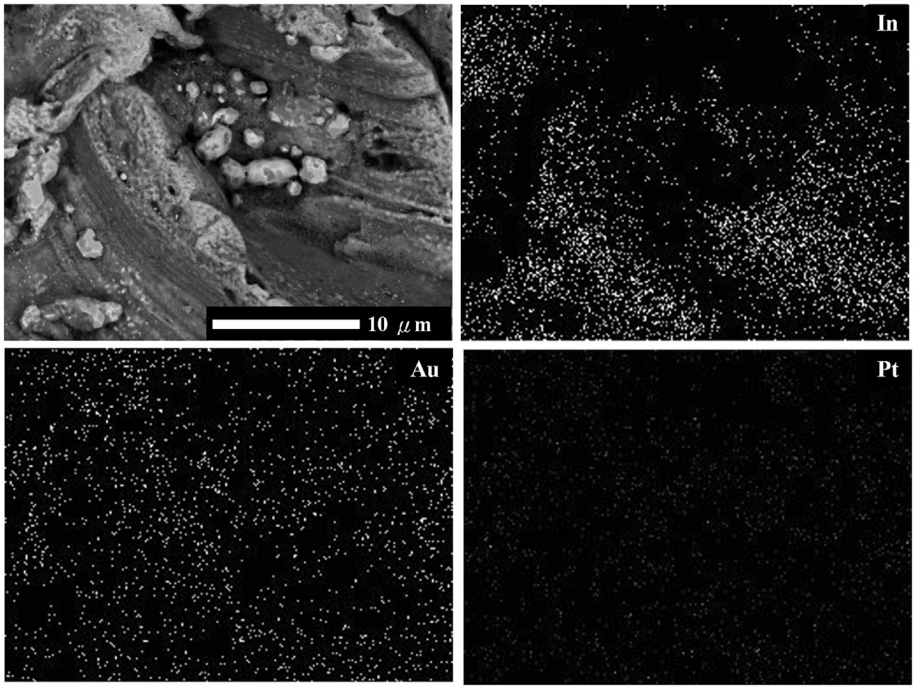

Figure 8 Backscattered electron image and energy-dispersive X-ray analysis maps showing element distributions of In, Au, and Pt.

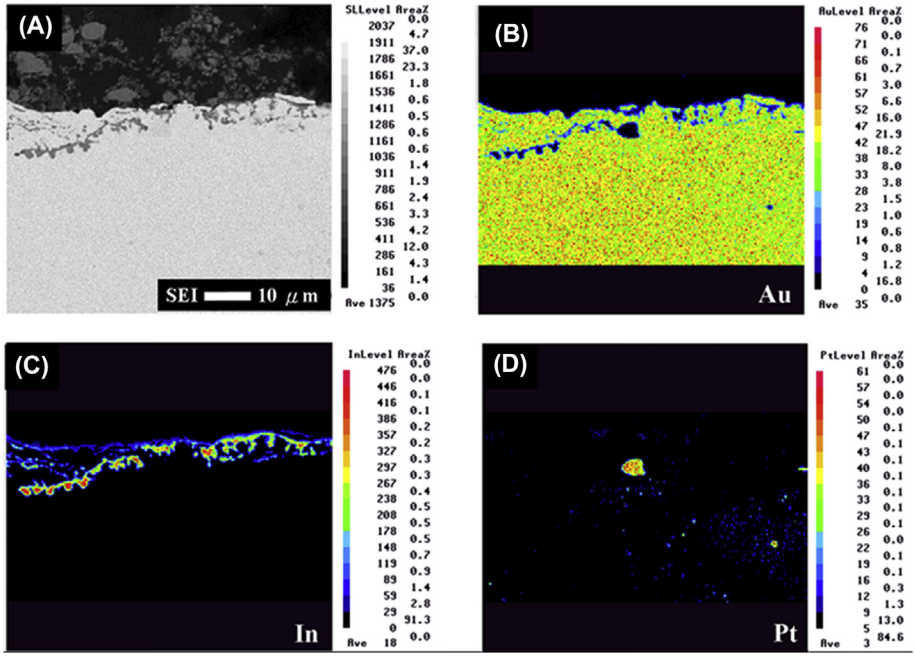

Figure 9 (A) Backscattered electron image micrograph and electron probe microanalysis color photomicrographs showing element distributions of (B) Au, (C) In, and (D) Pt between the interface of ceramic and metal after two porcelain-fused-to-metal firing cycles.

than the ceramic cohesive forces. Only In_2O_3 and Au were found on the alloy side of the interface, suggesting that In_2O_3 contributes to the interface bond strength. The results from this study are consistent with the findings of other studies.[5,11] Accumulation of easily oxidized elements at ceramic—metal interfaces has been reported in several studies to improve the adherence of porcelain to alloys of noble metals.[12—15,18—20] Such data are generally found to support the chemical bonding mechanisms.

In conclusion, In_2O_3 was found along the metal—ceramic interface from the results of XPS, EDX, and EPMA analysis. The presence of this oxide at the boundary promotes

metal—ceramic adhesion, and this resulted in initially cohesive failure in the ceramic layer. In_2O_3 is suggested to be beneficial for high fracture resistance of Au—Pt crown, which had the second highest fracture force in a previous fractural study of implant-supported crowns.[16]

Conflicts of interest

The authors have no conflicts of interest relevant to this article.

Acknowledgments

The authors gratefully acknowledge the School of Dentistry, National Yang-Ming University; Department of Materials and Optoelectronic Science, National Sun Yat-sen University; and the Department of Dentistry, Kaohsiung Veterans General Hospital for providing the resources for this study. We would like to thank all of the participants of this study. This study was supported by grants VGHNSU97-005 and VGHNSU98-003 from the Veterans Affairs Commission, Executive Yuan, R.O.C.

Appendix A. Supplementary data

Supplementary data related to this article can be found at http://dx.doi.org/10.1016/j.jds.2017.03.003.

References

1. Şahin S, Çehreli MC, Yalçın E. The influence of functional forces on the biomechanics of implant-supported prostheses—a review. *J Dent* 2002;30:271—82.
2. Çehreli M, Şahin S, Akça K. Role of mechanical environment and implant design on bone tissue differentiation: current knowledge and future contexts. *J Dent* 2004;32:123—32.
3. Miyata T, Kobayashi Y, Araki H, Ohto T, Shin K. The influence of controlled occlusal overload on peri-implant tissue. Part 3: a histologic study in monkeys. *Int J Oral Maxillofac Implants* 2000;15:425—31.
4. Isidor F. Loss of osseointegration caused by occlusal load of oral implants. A clinical and radiographic study in monkeys. *Clin Oral Implants Res* 1996;7:143—52.
5. Kinsel RP, Lin D. Retrospective analysis of porcelain failures of metal ceramic crowns and fixed partial dentures supported by 729 implants in 152 patients: patient-specific and implant-specific predictors of ceramic failure. *J Prosthet Dent* 2009;101:388—94.
6. Ucar Y, Brantley WA, Johnston WM, Iijima M, Han DS, Dasgupta T. Microstructure, elemental composition, hardness and crystal structure study of the interface between a noble implant component and cast noble alloys. *J Prosthet Dent* 2011;106:170—8.
7. Bagby M, Marshall SJ, Marshall Jr GW. Effects of porcelain application procedures on two noble alloys. *J Appl Biomater* 1990;1:31—7.
8. Papazoglou E, Brantley WA, Mitchell JC, Cai Z, Carr AB. New high-palladium casting alloys: studies of the interface with porcelain. *Int J Prosthodont* 1996;9:315—22.
9. Vrijhoef MMA, Van Der Zel JM. Oxidation of a gold—palladium PFM alloy. *J Oral Rehabil* 1988;15:307—12.
10. Hautaniemi JA, Heinonen M, Juhanoja J. Characterization of a surface-treated Au—Ag—Cu-based dental metal—ceramic alloy. *Surf Interface Anal* 1995;23:833—43.
11. Strub JR, Stiffler S, Schärer P. Cause of failure following oral rehabilitation: biological versus technical factors. *Quintessence Int* 1988;19:215—22.
12. Galindo DF, Ercoli C, Graser GN, Tallents RH, Moss ME. Effect of soldering on metal—porcelain bond strength in repaired porcelain-fused-to-metal casting. *J Prosthet Dent* 2001;85:88—94.
13. Park JS, Kim HS, Kim HSL, Son MK, Choe HC. Interfacial bonding and fracture phenomena between porcelain and metal coping. *Proced Eng* 2011;10:1567—72.
14. Kang MS, Ercoli C, Galindo DF, Graser GN, Moss ME, Tallents RH. Comparison of the load at failure of soldered and nonsoldered porcelain-fused-to-metal crown. *J Prosthet Dent* 2003;90:235—40.
15. Torrado E, Ercoli C, Al Mardini M, Graser GN, Tallents RH, Cordaro L. A comparison of the porcelain fracture resistance of screw-retained and cement-retained implant-supported metal-ceramic crowns. *J Prosthet Dent* 2004;91:532—7.
16. Chang HS, Chen M, Hsieh YD, Wu HJ. Fractural strength of porcelain fused to metal systems. *J Acad Oper Dent* 2011;2:11—22 [In Chinese, English abstract].
17. Chang HS, Yang CS, Hsieh YD, Chen M. Interfacial analysis of porcelain fused to high-palladium alloy with different observation methods. *J Dent Sci* 2016;11:156—63.
18. Briggs D, Seah MP, eds. *Practical Surface Analysis by Auger and X-Ray Photoelectron Spectroscopy*, 2nd ed. New York: Wiley, 1990.
19. Wagner CD. *Handbook of X-Ray Photoelectron Spectroscopy: A Reference Book of Standard Data for Use in X-Ray Photoelectron Spectroscopy*. Eden Prairie, MN: Perkin-Elmer Corp., 1979.
20. Lin AWC, Armstrong NR, Kuwana T. X-ray photoelectron/Auger electron spectroscopic studies of tin and indium metal foils and oxides. *Anal Chem* 1977;49:1228—35.
21. Brantley WA, Cai Z, Papazoglou E, et al. X-ray diffraction studies of oxidized high-palladium alloys. *Dent Mater* 1996;12:333—41.
22. Wu Y, Moser JB, Jameson LM, Malone WFP. The effect of oxidation heat treatment of porcelain bond strength in selected base metal alloys. *J Prosthet Dent* 1991;66:439—44.
23. Carpenter MA, Goodkind RJ. Effect of varying surface texture on bond strength of one semiprecious and one nonprecious ceramo-alloy. *J Prosthet Dent* 1979;42:86—95.
24. Wagner WC, Asgar K, Bigelow W, Flinn RA. Effect of interfacial variables on metal-porcelain bonding. *J Biomed Mater Res* 1993;27:531—7.
25. Okazaki M, Wang X, Toguchi MS, et al. Improvement of bond strength in metal-ceramic systems using a gold intermediate layer. *Dent Mater J* 1998;17:163—73.
26. Vasani R, Kawashima I, Ziebert GJ, Berzins DW. Metal-ceramic interface evaluation of a gold-infiltrated alloy. *J Prosthodont* 2009;18:560—5.
27. Carter JM, Al-Mudafar J, Sorensen SE. Adherence of a nickel-chromium alloy and porcelain. *J Prosthet Dent* 1979;41:167—72.
28. Papadopoulos T, Tsetsekou A, Eliades G. Effect of aluminium oxide sandblasting on cast commercially pure titanium surfaces. *Eur J Prosthodont Restor Dent* 1999;7:15—21.
29. Papadopoulos T, Tsetsekou A, Eliades G. Effect of Al_2O_3 sandblasting on casted cp Ti surfaces. *J Dent Res* 1998;77:1245.

30. Chang HS, Chen YS, Hsieh YD, Hsu ML. Stress distribution of two commercial dental implant systems: a three-dimensional finite element analysis. *J Dent Sci* 2013;8:261—71.
31. Shell JS, Nielsen JP. Study of the bond between gold alloys and porcelain. *J Dent Res* 1962;41:1424—37.
32. Mackert JR, Ringle RD, Parry EE, Evans AL, Fairhurst CW. The relationship between oxide adherence and porcelain-metal bonding. *J Dent Res* 1988;67:474—8.
33. Anusavice KJ. *Phillips' Science of Dental Materials*, 12th ed. St. Louis, MO: Saunders, 2012:377—82.